Simple Space-Domain Features for Low-Resolution sEMG Pattern Recognition

Ian M. Donovan, *Student Member, IEEE*, Juris Puchin, Kazunori Okada, *Member, IEEE*, and Xiaorong Zhang, *Member, IEEE*

***Abstract*—In recent years, low-cost, low-power myoelectric control systems such as the Myo armband from Thalmic Labs have become available and unlocked tremendous possibilities for myoelectric controlled applications. However, due to the embedded system constraints, such sEMG control devices typically samples sEMG signals at a lower frequency. It is in doubt whether existing sEMG feature extraction methods are still valid on such low-resolution sEMG data. In addition, the feature extraction algorithms implemented on embedded devices must have low computational complexity in order to meet the real-time requirement. This paper aims to investigate effective features for low-resolution EMG pattern recognition. In particular, a set of novel computational efficient space-domain (SD) features (referred to as simple SD (SSD) features) have been developed to exploit the spatial relationships of sEMG signals recorded from the sensor array on the Myo armband. The proposed SSD feature set was evaluated with a linear discriminant analysis (LDA)-based classifier on a 9-gesture dataset. The experimental results indicate that using the SSD features increased the classification accuracy by 5% compared to using Hudgins' time-domain features.**

I. Introduction

Surface electromyogram (sEMG) pattern recognition (PR) has been widely studied for identifying human movement intent in a large variety of applications, such as myoeletric-controlled prostheses [1-3], rehabilitation robotics [4], and gesture control interfaces [5]. Majority of these PR methods employ a similar processing sequence, which first segments raw signals into continuous analysis windows; then extracts characteristic features from each window; and finally concatenates features from individual channels into a feature vector and employs a classification method to classify the data. Common features used for sEMG characterization can be generally categorized into time-domain (TD) features (e.g. Hudgins' TD features [6]), frequency-domain features (e.g. autoregressive (AR)-based features), and time-frequency domain features (e.g. wavelet-derived features) [7]. TD features have been the most popular in real-time sEMG PR-controlled applications because of their relatively low computational requirements. Most of these feature extraction methods were developed based on high-quality sEMG signals sampled at a frequency of at least 1000 Hz. In addition, these existing methods mainly focus on extracting sEMG characteristics from individual sEMG channels without exploiting the relations between different channels, which are referred to as space-domain (SD) features.

The investigation on SD sEMG features has become more prevalent in recent years [8], but primarily with high-density (HD) sEMG electrodes [9]. HD sEMG electrodes have been mainly used for clinical diagnosis of neuromuscular diseases [10] and offline analysis of motor unit activities [11] because of its high computational burden.

With the advancement in embedded computer system design technology, low-cost, low-power sEMG control systems which seamlessly integrate sEMG sensing, embedded computing, and wireless communication into a small portable device have become available. One commercial solution is the Myo gesture control armband (Thalmic Labs) that integrates an ARM Cortex-M4 based microcontroller unit, eight sEMG sensors, an inertial measurement unit (IMU), and a Bluetooth Low Energy (BLE) module for wireless gesture control. Such EMG armband typically include multiple sEMG sensors arranged in a linear array on a flexible band which allows ease of wear in real life without the need of cumbersome anatomically targeted electrode placement. The emergence of these inexpensive, easy-to-wear devices has unlocked tremendous possibilities for myoelectric controlled applications. However, due to the embedded system constraints on data transmission bandwidth and power consumption, the Myo armband only samples sEMG signals at up to 200 Hz. It is in doubt whether existing sEMG feature extraction methods are still valid on such low resolution sEMG data. In addition, the feature extraction algorithms implemented on embedded devices must have low computational complexity in order to meet the real-time requirement.

This paper aims to investigate effective features for low resolution sEMG PR. In particular, a set of novel computational efficient SD features (referred to as simple SD (SSD) features) have been developed to exploit the spatial relationships of sEMG signals recorded from sensors arranged in an array which encompasses user's forearm with near equal spacing.

II. Methods

A. Data Collection

This study is conducted with Institutional Review Board (IRB) approval at San Francisco State University (SFSU) and informed consent of subjects. Our dataset includes sEMG data trials of nine complex hand gestures, including Fist Close, Hand Open, Index Point, Wave In, Wave Out, Thumb up,

This work is partly supported by the San Francisco State University (SFSU) Ken Fong Translational Research Fund, the SFSU Center for Computing for Life Sciences (CCLS) Mini Grant, and the California State University Program for Education & Research in Biotechnology (CSUPERB).

The authors are with SFSU, San Francisco, CA, 94132, USA. Corresponding author: Xiaorong Zhang (email: xrzhang@sfsu.edu).

Peace, Hang Loose, and Rock On (Figure 1), collected from 17 subjects on multiple days. Data acquisition was conducted using a Myo Armband worn on the subject's dominant forearm. Eight EMG signals were collected from the armband at the sampling rate of 200 Hz. The range of the digitized data is - 128 to +127 units with fidelity of 1 unit or approximately 3.5 uV.

The data was recorded using a software platform called MyoHMI [12] which facilitates the interface with a Myo armband and integrates a variety of signal processing modules as well as a graphic user interface. In the experiments, the MyoHMI prompts the subject with the gesture to perform. Each data trial consists of three repetitions of the gestures performed in sequence. Each gesture was performed for 2 seconds with 5 seconds rest time in-between. Totally 35 data trials were collected for this study. This includes 21 trials from seven subjects with three trials from each subject recorded on three different days, eight trials from four subjects with two trials from each subject, and six trials from six subjects with one trial per subject.

B. Feature Extraction

The raw sEMG data is segmented by overlapped analysis windows for feature extraction and pattern classification. The length and increment of the analysis window were set to 200ms (i.e. 40 samples) and 40ms (i.e. 8 samples) respectively as suggested in [13-14] for real-time control applications.

TD Features

The Hudgins' TD features [6] have been used extensively in real-time EMG PR for decades thus were used as a baseline in this study. Four TD features including mean absolute value (MAV), wavelength (Wave), zero crossings (Zeros), and sign slope changes (Turns) have been investigated. Due to the low sampling frequency of the sEMG signal, the fidelity of the two latter features are limited, as these features are the count of the number of times the signal crosses zero or the slope of the waveform changes sign. Also, a threshold of 3 units was used when calculating Zeros and Turns for all reported results to reduce the noise induced. This value was found to maximize classification accuracies for models based on these features alone in our experiments.

SD Features

The MAV is primarily affected by which muscles are contracted when a gesture is being performed as well as the force the subject is using to produce the gesture, or gesture intensity (i.e. weak fist verse strong fist). For each window, the MAV calculated from the i^{th} channel can be expressed as

$$MAV_i = \frac{\sum_{n=1}^{wl} |x_i[n]|}{wl}$$

where wl is the window length, or the number of raw data points in one window, and $x_i[n]$ denotes the n^{th} raw data point from the i^{th} channel. If it is assumed that the local intensity of an individual sEMG signal changes linearly proportional to the intensity of the gesture, then scaling the MAV of each channel by the average MAV across all channels should remove the dependency of gesture intensity. The averaged MAV across all channels is referred to as the Mean MAV (MMAV), which can be calculated as

$$MMAV = \frac{\sum_{i=1}^{8} MAV_i}{8}$$

The MAV scaled by the MMAV is referred to as Scaled MAV (SMAV). For each window, the SMAV extracted from the i^{th} channel is expressed as

$$SMAV_i = \frac{MAV_i}{MMAV}.$$

The SMAV represents a non-dimensional relationship between the channels. For uses in LDA and similar classifiers, it should be noted that one independent variable is lost among the eight SMAVs extracted from individual channels because the sum of the SMAVs of all channels equals one by the definition. As all inputs to these classifiers need to be independent, the SMAV from one of channels was replaced by the MMAV in our experiments.

Each sensor located around the perimeter of the arm represents a mixture of sources. Individual sources can affect multiple sensors depending on the size and location of the source. Sources affecting multiple sensors will increase the correlation across those sensors, whereas more focused sources primarily affecting only one sensor will decrease the correlation. Therefore, for each window the correlation coefficient (CC) between channel i and its neighboring channel $i+1$ is calculated as

$$CC_i = \frac{\sum_{n=1}^{wl} X_i[n]X_{i+1}[n]}{\sum_{n=1}^{wl} X_i[n]^2} = \frac{\sum_{n=1}^{wl} X_i[n]X_{i+1}[n]}{wl}$$

where $X_i[n]$ is the n^{th} data point from channel i after the data in the window is normalized. For normalization, each window of data first has its mean value subtracted from each raw data point, and then the resulting values are divided by their standard deviation.

To further decrease the computational complexity of the CC feature which involves a series of multiplication operations, mean absolute difference (MAD)-based features are proposed in this study, which also characterizes spatial relations between channels with lower computational complexities. The

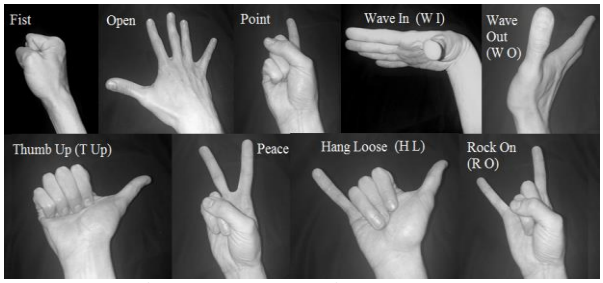

Figure 1. Classified nine gestures. Left to right, top to bottom: Fist Close, Hand Open, Index Point, Wave In, Wave Out, Thumb Up, Pease, Hang Loose, and Rock On

MAD features include the mean absolute difference of the normalized values (MADN), which can be calculated as

$$MADN_i = \frac{\sum_{n=1}^{wl} |X_i[n] - X_{i+1}[n]|}{\sum_{n=1}^{wl} X_i[n]^2} = \frac{\sum_{n=1}^{wl} |X_i[n] - X_{i+1}[n]|}{wl}.$$

Both CC and MADN require normalization of the windows before extraction. Instead, taking the MAD of the raw signal (MADR) eliminates this requirement. The MADR of channel i is calculated as

$$MADR_i = \frac{\sum_{n=1}^{wl} |x_i[n] - x_{i+1}[n]|}{wl}.$$

This value is affected by gesture intensity, so finally the MAD of the raw signal scaled by MMAV (referred to as scaled MADR (SMADR)) is proposed to remove the dependency of gesture intensity. The SMADR of channel i is expressed as

$$SMADR_i = \frac{MADR_i}{MMAV}$$

It is notable that MADN, MADR, and SMADR are inversely related to correlation, and can be instead viewed as a measure of uniqueness.

SSD Feature Set

In this paper, the combination of the SMAV feature as well as the MAD features is referred to as the SSD feature set because of their spatial characteristics as well as mathematical simplicity.

C. Validation and Testing

Evaluation of the effectiveness of these feature extraction methods was based on the resulting accuracies from classification. A simple LDA classifier was adopted in this study for pattern classification because of its previous success in EMG PR and its computational efficiency for real-time processing. For each data trial, the data was divided into six subsets. An LDA model was trained from each subset and then tested on the remaining five subsets, resulting in six classification accuracies. The average classification accuracy was then calculated for each data trial.

III. RESULTS

The tables in this section show the averaged classification accuracies (ACAs) and the standard deviations (STDs) across all 35 data trials.

A. Classification Results with Hudgins' TD Features

The four TD features have first been used separately for pattern classification in order to quantify their individual ability to discriminate gestures. As seen in Table I, the MAV has resulted in the highest ACA. Combinations of MAV with the other three features have also been analyzed, but using MAV alone still outperforms all investigated combinations.

B. Classification Results with SD Features

As shown in Table II, using SMAV instead of MAV has boosted the ACA by more than 2%. Similarly, using SMAV alone has yielded better performance than combining it with other TD features.

Table III shows the results of exploiting the SD features. The CC and MADN features alone have resulted in low ACAs similar to Zeros and Turns; however, instead of decreasing the ACAs when combined with SMAV like the TD features have done, the CC and MAD features have improved the ACAs.

The MADN has resulted in slightly higher ACA than the CC feature while having lower computational requirement. As can be seen in the table, the combination of SMAV and MADN has resulted in the best ACA. The ACA provided by the SMAV and SMADR combination is only about 1% less accurate than the SMAV and MADN combination. But the SMADR feature is more computational efficient than the MADN as it does not require normalization.

C. Confusion Matrices

TABLE I. CLASSIFICATION RESULTS WITH HUDGINS' TD FEATURES

Features Used	ACA	STD
MAV	77.52%	6.68%
Wave	75.27%	7.07%
Zeros	58.14%	11.91%
Turns	50.24%	12.86%
MAV, Wave	76.80%	6.70%
MAV, Zeros	76.74%	6.97%
MAV, Turns	76.84%	6.61%
MAV, Wave, Zeros	76.24%	6.83%
MAV, Zeros, Turns	75.88%	7.07%
MAV, Wave, Turns	76.47%	6.66%
MAV, Wave, Zeros, Turns	75.59%	6.84%

TABLE II. CLASSIFICATION RESULTS WITH THE SMAV FEATURE

Features Used	ACA	STD
MAV	77.52%	6.68%
MAV, Wave, Zeros, Turns	75.59%	6.84%
SMAV	79.70%	6.46%
SMAV, Wave, Zeros, Turns	76.64%	6.56%

TABLE III. CLASSIFICATION RESULTS WITH SD FEATURES

Features Used	ACA.	STD
SMAV	79.70%	6.46%
CC	52.31%	10.90%
MADN	53.47%	11.12%
MADR	73.45%	7.59%
SMADR	76.57%	7.81%
SMAV, CC	82.03%	6.79%
SMAV, MADN	82.43%	6.56%
SMAV, MADR	80.20%	6.20%
SMAV, SMADR	81.46%	6.47%

Tables IV and V show the between-gesture confusion matrices of the ACAs derived from the TD features (MAV alone) and from the SSD features (SMAV+MADN), respectively. The rows are the true gestures being performed and the columns are the resulting classification decisions.

Analyzing the confusion matrixes, the 'Fist' and 'Thumb Up' gestures have the highest confusion (~10%). 'Point' is also confused with both of these gestures (~5%). All three of these gestures include the flexing of the middle, ring, and pinky fingers. 'Hand Open, 'Peace', 'Hang Loose' and 'Rock On' all involve the extension of fingers. 'Thumb Up' and 'Hang Loose' are also similar only differing with a pinky extension. These groups of similar gestures corresponded to the highest confusion rates. As can be seen in the tables, the replacement of TD features with SSD features has decreased most of the confusion rates.

IV. Conclusion

This paper has investigated the effectiveness of two sets of features for low-resolution sEMG PR. The first set is the commonly used Hudgins' TD features and the second set is the newly proposed SSD features. The experimental results have shown that not all four of the Hudgins' TD features are effective for low-resolution sEMG PR. The inclusion of Zeros and Turns actually dropped the overall ACAs. This may be due to the low temporal resolution of the sEMG signals collected from the Myo Armband. Compared to the TD features, the use of the proposed SSD feature set that combines the SMAV and the MAD features has been shown to increase the ACAs by up to 5%. In addition, the SSD features are all mathematically simple, which are essential for real-time computing on embedded systems. The proposed SSD features have the potential of improving accuracies in other EMG PR-based applications as well. Future work includes evaluating the SSD features in real-time experiments and investigating the effectiveness of SSD features in HD sEMG systems.

TABLE IV. CONFUSION MATRIX OF ACAS (%) DERIVED FROM TD FEATURES

	Fist	Open	Point	W I	W O	T Up	Peace	H L	R O
Fist	74.4	0.9	7.7	0.9	1.0	12.6	1.2	0.4	1.0
Open	1.0	69.7	3.4	0.7	3.3	3.0	5.6	7.1	6.2
Point	4.9	3.0	68.0	1.4	0.0	9.1	4.5	2.6	6.4
W I	1.3	1.7	3.3	84.9	0.8	2.2	2.5	2.3	1.0
W O	0.6	3.6	0.0	0.7	88.0	0.1	3.6	1.9	1.4
T Up	7.3	1.7	8.3	0.7	0.1	74.9	1.2	5.3	0.6
Peace	0.6	4.2	4.4	1.0	3.0	1.1	66.8	10.7	8.2
H L	0.4	4.8	2.2	0.5	0.9	4.8	8.7	75.3	2.5
R O	0.5	4.4	6.1	0.4	1.4	0.4	6.8	1.7	78.3

TABLE V. CONFUSION MATRIX OF ACAS (%) DERIVED FROM SSD FEATURES

	Fist	Open	Point	W I	W O	T Up	Peace	H L	R O
Fist	82.1	1.1	3.7	0.8	0.6	9.5	1.5	0.4	0.3
Open	1.1	76.8	2.0	0.6	2.3	2.5	5.3	4.0	5.5
Point	4.2	2.3	76.4	1.5	0.0	6.8	2.7	1.9	4.2
W I	0.9	1.3	2.2	89.6	0.5	1.2	2.4	1.5	0.4
W O	0.3	1.9	0.0	0.4	95.0	0.0	1.2	0.6	0.5
T Up	8.6	1.0	4.1	0.3	0.1	80.4	0.5	4.3	0.5
Peace	0.4	3.7	2.7	0.7	2.3	0.1	74.3	8.8	7.0
H L	0.1	3.5	1.2	0.2	0.7	2.9	7.3	82.7	1.4
R O	0.2	3.8	3.5	0.2	1.4	0.2	4.7	1.5	84.5

References

[1] Kuiken TA, Li G, Lock BA, Lipschutz RD, Miller LA, Stubblefield KA, Englehart KB: **Targeted muscle reinnervation for real-time myoelectric control of multifunction artificial arms.** *Jama* 2009, **301:**619-628.

[2] Parker P, Englehart K, Hudgins B: **Myoelectric signal processing for control of powered limb prostheses.** *Journal of electromyography and kinesiology: official journal of the International Society of Electrophysiological Kinesiology* 2006, **16:**541.

[3] Zhang X, Liu Y, Zhang F, Ren J, Sun YL, Yang Q, Huang H: **On Design and Implementation of Neural-Machine Interface for Artificial Legs.** *Industrial Informatics, IEEE Transactions on* 2012, **8:**418-429.

[4] Cesqui B, Tropea P, Micera S, Krebs HI: **EMG-based pattern recognition approach in post stroke robot-aided rehabilitation: a feasibility study.** *Journal of neuroengineering and rehabilitation* 2013, **10:**75.

[5] Saponas TS, Tan DS, Morris D, Turner J, Landay JA: **Making muscle-computer interfaces more practical.** In *Proceedings of the SIGCHI Conference on Human Factors in Computing Systems*. ACM; 2010: 851-854.

[6] Hudgins B, Parker P, Scott RN: **A new strategy for multifunction myoelectric control.** *Biomedical Engineering, IEEE Transactions on* 1993, **40:**82-94.

[7] Oskoei MA, Hu H: **Myoelectric control systems—A survey.** *Biomedical Signal Processing and Control* 2007, **2:**275-294.

[8] Rahimi A, Benatti S, Kanerva P, Benini L, Rabaey JM: **Hyperdimensional biosignal processing: A case study for EMG-based hand gesture recognition.** In *Rebooting Computing (ICRC), IEEE International Conference on*. IEEE; 2016: 1-8.

[9] Stango A, Negro F, Farina D: **Spatial correlation of high density EMG signals provides features robust to electrode number and shift in pattern recognition for myocontrol.** *IEEE Transactions on Neural Systems and Rehabilitation Engineering* 2015, **23:**189-198.

[10] Drost G, Stegeman DF, van Engelen BG, Zwarts MJ: **Clinical applications of high-density surface EMG: a systematic review.** *Journal of Electromyography and Kinesiology* 2006, **16:**586-602.

[11] Merletti R, Holobar A, Farina D: **Analysis of motor units with high-density surface electromyography.** *Journal of Electromyography and Kinesiology* 2008, **18:**879-890.

[12] Donovan I, Valenzuela K, Ortiz A, Dusheyko S, Jiang H, Okada K, Zhang X: **MyoHMI: A low-cost and flexible platform for developing real-time human machine interface for myoelectric controlled applications.** In *Systems, Man, and Cybernetics (SMC), 2016 IEEE International Conference on*. IEEE; 2016: 004495-004500.

[13] Smith LH, Hargrove LJ, Lock BA, Kuiken TA: **Determining the optimal window length for pattern recognition-based myoelectric control: balancing the competing effects of classification error and controller delay.** *Neural Systems and Rehabilitation Engineering, IEEE Transactions on* 2011, **19:**186-192.

[14] Farrell TR, Weir RF: **The optimal controller delay for myoelectric prostheses.** *IEEE Transactions on Neural Systems and Rehabilitation Engineering* 2007, **15:**111-118.